Available online at www.sciencedirect.com
ScienceDirect
Journal of Sound and Vibration 313 (2008) 246–267
JOURNAL OF SOUND AND VIBRATION
www.elsevier.com/locate/jsvi

Large-amplitude dynamic analysis of simply supported skew plates by a variational method

Debabrata Das, Prasanta Sahoo*, Kashinath Saha

Department of Mechanical Engineering, Jadavpur University, Kolkata 700032, India

Received 30 May 2007; received in revised form 21 August 2007; accepted 17 November 2007
Available online 4 March 2008

Abstract

Large-amplitude free vibration analysis of simply supported thin isotropic skew plates has been presented. The large deformation is imparted statically by subjecting the plate under uniform transverse pressure. The mathematical formulation is based on the variational principle in which the displacement fields are assumed as a combination of orthogonal polynomial or transcendental functions, each satisfying the corresponding boundary conditions of the plate. The large-amplitude dynamic problem is addressed by solving the corresponding static problem first, and subsequently with the resultant displacement field, the problem is formulated. The vibration frequencies are obtained from the solution of a standard eigenvalue problem. Entire computational work is carried out in a normalized square domain obtained through an appropriate domain mapping technique. Results of the reduced problem revealed excellent agreement with other studies and a typical comparison of the actual problem is also carried out successfully. Results are furnished in dimensionless amplitude–frequency plane, in the form of backbone curves and pictorial representations of some vibration mode shapes are made.

1. Introduction

Linear free vibration analysis of a structure is carried out to predict the inherent dynamic response of the structure on which modern-day design practices are based. However, large-amplitude vibration frequencies of a structure are expected to change significantly from its linear counterparts because of the fact that the stiffness of a deformed structure changes appreciably due to the effect of geometric nonlinearity. This effect is found to be more prominent in case of the structural elements under large static deformation. Predicting the large-deformation free vibration response of structural elements is a challenging task even to the present-day researchers. In the present paper, the study of the large deformation free vibration analysis of skew plates has been presented. Skew plates have quite a good number of applications in civil, aerospace and other forms of structures.

Prathap and Varadan [1] studied the large-amplitude free flexural vibrations of thin, elastic anisotropic skew plates using the von Karman field equations. Naturally, the governing nonlinear dynamic equations are

*Corresponding author. Tel./fax: +91 33 2414 6890.
E-mail address: psahoo@vsnl.net (P. Sahoo).

0022-460X/$ - see front matter © 2007 Elsevier Ltd. All rights reserved.
doi:10.1016/j.jsv.2007.11.036

Nomenclature

a	length of the plate
b	oblique width of the plate
$\{\mathbf{d}\}$	vector of unknown coefficients
D	flexural rigidity of the plate
E	Young's modulus of the plate material
$\{\mathbf{f}\}$	load vector
$\mathbf{J}$	Jacobian of the coordinate transformation
$[\mathbf{k}^b]$	part of stiffness matrix coming from the bending action
$[\mathbf{k}^m]$	part of stiffness matrix coming from the membrane forces
$[\mathbf{K}]$	stiffness matrix
$[\mathbf{M}]$	mass matrix
n_u	number of functions for displacement field u
n_v	number of functions for displacement field v
n_w	number of functions for displacement field w
p	uniformly distributed transverse load
P	concentrated transverse load
t	thickness of the plate
u	displacement along the x-direction
U	strain energy
U^b	strain energy due to flexural action
U^m	strain energy due to membrane action
v	displacement along the y-direction
V	work potential
w	transverse displacement
w^*	dimensionless maximum transverse displacement ($= w_{\max}/t$)
α_i	set of functions defining approximate displacement field u
β_i	set of functions defining approximate displacement field v
γ_i	set of temporal functions
η	normalized coordinates in the y-direction
θ	skew angle
λ	dimensionless frequency parameter
ν	Poisson's ratio
ξ	normalized coordinates in x-direction
ρ	density of plate material
τ	time
ϕ_i	set of functions defining approximate displacement field w
ω	natural frequency
ω_1	fundamental linear frequency
ω_{nl}	nonlinear frequency

derived in terms of stress function and lateral displacement and they obtained the solutions by the Galerkin method on the basis of a one-term assumed vibration mode. Liew and Lam [2] studied the flexural vibration of skew plates by the Rayleigh–Ritz method (RRM) using a set of admissible two-dimensional orthogonal plate functions satisfying boundary conditions. They used the Gram–Schmidt orthogonalization procedure to generate higher-order terms in the two-dimensional orthogonal plate functions. The natural vibrations of thick and thin rhombic plates with clamped and simply supported edges have been analysed by McGee et al. [3] using assemblages of nine-node Lagrangian isoparametric quadrilateral C^0 continuous finite elements based on a higher-order shear-deformable thick plate theory. Additional nodal displacement degrees of freedom are derived by retaining higher-order powers of the thickness coordinate in the in-plane displacement fields, which in turn allows for the proper representation of the transverse shear strains of thick plates. Singh and Chakraverty [4] used RRM to determine the flexural vibration frequencies of skew plates and utilized the Gram–Schmidt orthogonalization procedure to generate the admissible set of polynomial functions from the prescribed start function.

Using the first-order shear deformation plate theory, Wang [5] presented a B-spline RRM for free vibration analysis of skew fibre-reinforced composite laminates, which may have arbitrary lay-ups, admitting the possibility of coupling between in-plane and out-of-plane behaviour and genera1 anisotropy. In this approach, the displacement field consists of three mid-surface translational displacements u, v, and w and two through-thickness shear strains instead of two rotations in order to avoid the shear locking phenomenon. The RRM has been used by Singh and Saxena [6] to study the transverse vibrations of skew plates of variable thickness with different combinations of boundary conditions at the four edges. In this paper, the two-dimensional thickness variations are taken as the Cartesian product of linear variations along the two concurrent edges of the plate. Žitňan [7] studied the transverse vibrations of rectangular and skew plates by the RRM using

B-spline trial functions. Reddy and Palaninathan [8] have extended the use of a general high-precision triangular plate bending finite element to the free vibration analysis of laminated skew plates by deriving the consistent mass matrix in an explicit form. They imposed boundary conditions on the skew edges through the transformed element matrices. Saadatpour et al. [9] considered a theoretical formulation for the dynamic analysis of simply supported quadrilateral plates having intermediate line and point supports. They used natural coordinates in conjunction with the Galerkin method to provide one single super-element in order to represent the whole plate. Mizusawa and Kondo [10] used the spline element method to analyse the vibration of isotropic, skew Mindlin plates of varying thickness.

Singha and Ganapathi [11] investigated large-amplitude free flexural vibration behaviours of thin laminated composite skew plates using the finite element approach, considering the effect of shear deformation, in-plane and rotary inertia. They used von Karman's assumptions to introduce geometric nonlinearity. The nonlinear governing equations are obtained by employing Lagrange's equations of motion and are solved using the direct iteration technique. A meshfree method based on the reproducing kernel particle approximate is employed by Liew et al. [12] for the free vibration and buckling analyses of shear-deformable plates. In this approach, the first-order Mindlin/Reissner plate theory is used, and the displacement shape functions are constructed using the reproducing kernel approximation satisfying the consistency condition. An examination of the accuracy and convergence behaviours of polynomial basis function differential quadrature and harmonic basis function differential quadrature for free vibration analysis of variable-thickness thick skew plates has been carried out by Malekzadeh and Karami [13], where the plate governing equations are based on the first-order shear deformation theory including the effects of rotary inertia. They employed arbitrary thickness variations, yielding a system of equations with nonlinear spatial-dependent coefficients. Zhou et al. [14] studied the free vibration characteristics of skew thick plates with arbitrary boundary conditions based on three dimensional, linear, and small strain elasticity theory. They derived the eigenvalue equation from the energy functional of the plate by using the Ritz method and developed the trial functions of the displacement components from a set of triplicate Chebyshev polynomial series multiplied by a boundary function chosen to satisfy the essential geometric boundary conditions of the plate. Singh and Tanveer [15] carried out the analysis by the p-type variational method and have reported some results for the linear dimensionless frequency parameters for rhombic skew plates.

In the present work, a simulation model for large-deformation free vibration analysis of a thin isotropic skew plate has been presented. The mathematical formulation is based on variational form of energy principle. To predict the large-amplitude vibration frequency of the plate, first a static analysis is carried out and then knowing the deformed shape, an eigenvalue problem is formulated corresponding to the system stiffness. A good number of results has been presented, which will be of great help to the designers.

2. Mathematical formulation

A skew plate ($a \times b \times t$) with skew angle θ is shown in Fig. 1. The mathematical formulation is based on the assumption that the material of the plate is isotropic and homogeneous and obeys linear elastic stress–strain relation. The thickness of the plate is considered to be sufficiently small so as to avoid the effect of shear deformation. Also, the stress and strain measures are based on the original dimension of the plate.

2.1. Mapping of the physical domain into the computational domain

The physical domain of interest in the x–y coordinate system shown in Fig. 1 is mapped to the computational domain in the $\xi - \eta$ coordinate system as shown in Fig. 2. In the computational domain, the constant ξ and constant η lines are selected at the Gauss points. The x–y coordinates of all the Gauss points in the computational domain are calculated by suitable grid generation techniques.

2.2. Static analysis

It is well known that nonlinear vibration frequency is amplitude dependent and establishment of the particular relationship is the primary objective of any large-amplitude vibration analysis. With increase

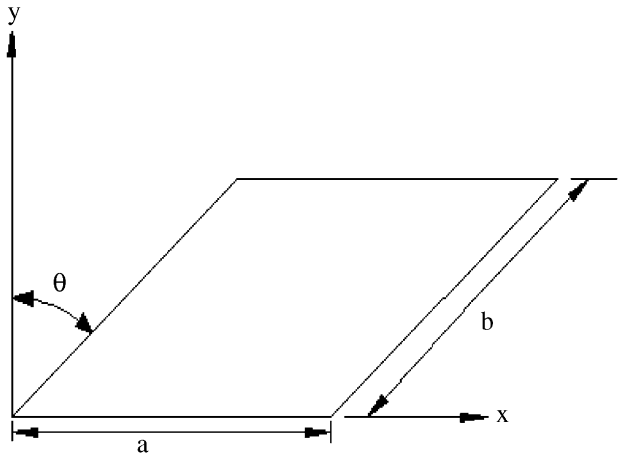

Fig. 1. Skew plate in x–y plane.

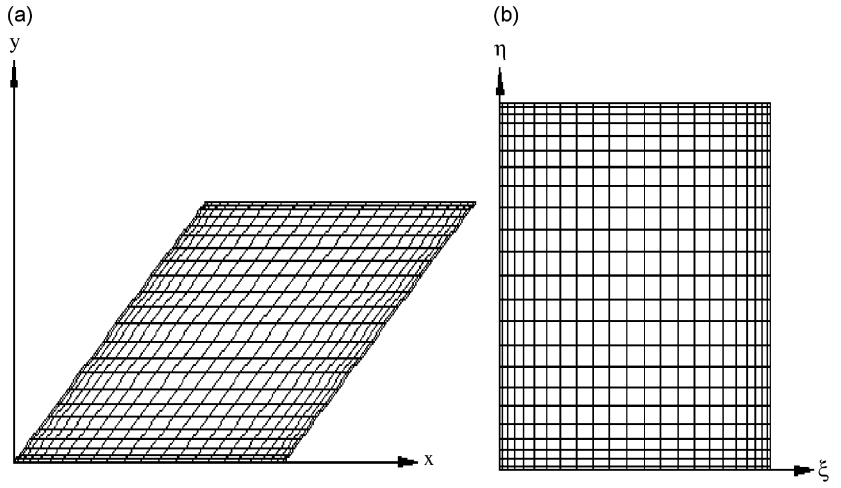

Fig. 2. Gauss point locations for skew plate: (a) physical domain and (b) computational domain.

in vibration amplitude, strain energy stored in the plate increases, thus changing its dynamic behaviour. In the present work, analysis is carried out in two parts: first the problem corresponding to the transverse loading is solved and subsequently the dynamic problem is taken up with the known displacement field.

2.2.1. Variational form of equations

The variational principle states that

$$\delta(U + V) = 0, \tag{1}$$

where $U(= U^b + U^m)$ is the total strain energy, U^b the strain energy due to pure bending and U^m the strain energy due to stretching of its middle surface, and V the potential of the external forces. The expressions for U^b and U^m have been mentioned in an earlier study [16] for rectangular plates and their expressions for a skew plate is indicated here once again.

U^b is given by

$$U^b = \frac{D}{2}\int_0^{b\cos\theta}\int_{y\tan\theta}^{y\tan\theta+a}\left[\left\{\left(\frac{\partial^2 w}{\partial x^2}\right)^2+\left(\frac{\partial^2 w}{\partial y^2}\right)^2+2\frac{\partial^2 w}{\partial x^2}\frac{\partial^2 w}{\partial y^2}\right\}-2(1-v)\left\{\frac{\partial^2 w}{\partial x^2}\frac{\partial^2 w}{\partial y^2}-\left(\frac{\partial^2 w}{\partial x\,\partial y}\right)^2\right\}\right]\mathrm{d}x\,\mathrm{d}y, \tag{2}$$

where $D = Et^3/(12(1-v^2))$ is the flexural rigidity of the plate, and u, v, and w are displacements along the x-, y-, and z-directions, respectively.

U^m is given by

$$\begin{aligned} U^m = \frac{Et}{2(1-v^2)}\int_0^{b\cos\theta}\int_{y\tan\theta}^{y\tan\theta+a}\Bigg[&\left\{\left(\frac{\partial u}{\partial x}\right)^2+\left(\frac{\partial v}{\partial y}\right)^2+\frac{\partial u}{\partial x}\left(\frac{\partial w}{\partial x}\right)^2+\frac{\partial v}{\partial y}\left(\frac{\partial w}{\partial y}\right)^2\right\}+\frac{1}{4}\left\{\left(\frac{\partial w}{\partial x}\right)^2+\left(\frac{\partial w}{\partial y}\right)^2\right\}^2\\ &+2v\left\{\frac{\partial u}{\partial x}\frac{\partial v}{\partial y}+\frac{1}{2}\frac{\partial v}{\partial y}\left(\frac{\partial w}{\partial x}\right)^2+\frac{1}{2}\frac{\partial u}{\partial x}\left(\frac{\partial w}{\partial y}\right)^2\right\}+\frac{1-v}{2}\left\{\left(\frac{\partial u}{\partial y}\right)^2+\left(\frac{\partial v}{\partial x}\right)^2+2\frac{\partial u}{\partial y}\frac{\partial v}{\partial x},\right.\\ &\left.+2\left(\frac{\partial u}{\partial y}+\frac{\partial v}{\partial x}\right)\frac{\partial w}{\partial x}\frac{\partial w}{\partial y}\right\}\Bigg]\mathrm{d}x\,\mathrm{d}y. \end{aligned} \tag{3}$$

For a plate loaded with uniform transverse pressure p and a concentrated load P, potential energy V is given by

$$V = -\int_0^{b\cos\theta}\int_{y\tan\theta}^{y\tan\theta+a}(pw)\,\mathrm{d}x\,\mathrm{d}y - Pw|_{x,y}, \tag{4}$$

where $w|_{x,y}$ is deflection of the concentrated load application point.

2.2.2. Approximate displacement field

The displacement fields w, u, and v are expressed by linear combinations of unknown parameters d_i as follows:

$$w(\xi,\eta)=\sum_{i=1}^{n_w} d_i\phi_i(\xi,\eta),\quad u(\xi,\eta)=\sum_{i=n_w+1}^{n_w+n_u} d_i\alpha_{i-n_w}(\xi,\eta),\quad v(\xi,\eta)=\sum_{i=n_w+n_u+1}^{n_w+n_u+n_v} d_i\beta_{i-n_w-n_u}(\xi,\eta), \tag{5}$$

where $\phi(\xi,\eta)$, $\alpha(\xi,\eta)$, and $\beta(\xi,\eta)$ are sets of orthogonal functions and n_w, n_u, and n_v are numbers of functions for w, u, and v, respectively.

The start functions of these orthogonal sets are selected to satisfy the flexural and membrane boundary conditions of the plate. To cater to the need of the numerical scheme, all the start functions are defined in the computational domain. The basis functions for the definition of plate deflection w comes from the flexural simply supported boundary condition. The start functions for u and v are selected to satisfy the zero-displacement boundary conditions at the boundary edges. Although the present paper deals with simply supported boundary condition, the result for any boundary condition may also be obtained by selecting the appropriate flexural plate deflection function.

The higher-order functions are generated following a two-dimensional implementation of the Gram–Schmidt scheme. In the conventional method of generating higher-order functions, first the higher-order one-dimensional functions are generated from the corresponding start functions and then two-dimensional functions are generated by ordered multiplication of the one-dimensional functions corresponding to two orthogonal directions. But the present method is based on the functions generated by the two-dimensional implementation of the Gram–Schmidt scheme. In this method, higher-order functions corresponding to a particular orthogonal direction are first generated through the Gram–Schmidt scheme, for a fixed coordinate value of the other orthogonal axis. Then each of these functions is treated as start functions to generate the complete set of higher-order two-dimensional functions. The advantage of using this technique is that unlike the earlier case, the basis functions can be of two variables, which are not separable in the individual spatial coordinates.

2.2.3. Governing system of equations

Using Eqs. (2)–(5) in Eq. (1), the governing equations are obtained in the following form:

$$[\mathbf{K}]\{\mathbf{d}\} = \{\mathbf{f}\}, \tag{6}$$

where $[\mathbf{K}] = [\mathbf{k}^b] + [\mathbf{k}^m]$ is the total stiffness matrix, $[\mathbf{k}^b]$ and $[\mathbf{k}^m]$ being the contribution from bending and stretching action and $\{\mathbf{d}\}$ is the unknown coefficient vector. In the right-hand side of the equation, $\{\mathbf{f}\}$ is the load vector and it is to be noted that the dimensions of all the matrices and vectors are $(n_w + n_u + n_v)$. Details of the stiffness matrices and load vector are provided in the Appendix.

2.2.4. Solution of the static displacement field

The set of governing equations (Eq. (6)) is nonlinear in nature and solved by the direct substitution technique using the successive relaxation scheme [17]. For each load step, the values of $\{\mathbf{d}\}$ are assumed to evaluate the stiffness matrix. Using the stiffness matrix, based on assumed values, new values of $\{\mathbf{d}\}$ are calculated by the matrix inversion technique from the expression $\{\mathbf{d}\} = [\mathbf{K}]^{-1}\{\mathbf{f}\}$. Calculated values of $\{\mathbf{d}\}$ are compared with their values in the previous iteration. If the difference comes below a predefined value of error limit ε, the convergence of deflection field is assumed, otherwise the values of $\{\mathbf{d}\}$ are modified with a relaxation parameter and it is taken as the next approximation for the values of $\{\mathbf{d}\}$. Once a solution is obtained for a load, an increment is given on the load and iteration starts with the present solution. In the present extrapolation technique, another assumed deflection field has also been extrapolated from the previous solution set using the ratios of the unknown coefficients $\{\mathbf{d}\}$ for the preceding two load steps. Although this technique has not been tried extensively, this can be utilized as a useful numerical tool for the solution of a nonlinear set of equations, when convergence becomes difficult.

2.3. Dynamic analysis

The variational form of the dynamic problem is derived from Hamilton's principle, which states that

$$\delta\left(\int_{\tau_1}^{\tau_2} L\,\mathrm{d}\tau\right) = 0, \tag{7}$$

where $L = T - (U + V)$ is called the Lagrangian and T, U, and V are the total kinetic energy, strain energy and potential of the external forces, respectively.

The mathematical expressions of U and V have already been given in Eqs. (2) and (3), respectively, and the kinetic energy T is expressed as

$$T = \frac{1}{2}\rho t \int_0^{b\cos\theta} \int_{y\tan\theta}^{y\tan\theta+a} \left(\left(\frac{\partial w}{\partial \tau}\right)^2 + \left(\frac{\partial u}{\partial \tau}\right)^2 + \left(\frac{\partial v}{\partial \tau}\right)^2\right) \mathrm{d}x\,\mathrm{d}y. \tag{8}$$

In the normalized plane, T is given by

$$T = \frac{1}{2}\rho t \int_0^1 \int_0^1 \left(\left(\frac{\partial w}{\partial \tau}\right)^2 + \left(\frac{\partial u}{\partial \tau}\right)^2 + \left(\frac{\partial v}{\partial \tau}\right)^2\right) \det \mathbf{J}\,\mathrm{d}\xi\,\mathrm{d}\eta.$$

2.3.1. Governing system of equations

The dynamic displacements $w(\xi,\eta,\tau)$, $u(\xi,\eta,\tau)$, and $v(\xi,\eta,\tau)$ are assumed to be separable in space and time as shown below:

$$w(\xi,\eta,\tau) = \sum_{i=1}^{n_w} d_i \phi_i(\xi,\eta)\gamma_i(\tau),$$

$$u(\xi,\eta,\tau) = \sum_{i=n_w+1}^{n_w+n_u} d_i \alpha_{i-n_w}(\xi,\eta)\gamma_{i-n_w}(\tau),$$

$$v(\xi,\eta,\tau)=\sum_{i=n_w+n_u+1}^{n_w+n_u+n_v} d_i\beta_{i-n_w-n_u}(\xi,\eta)\gamma_{i-n_w-n_u}(\tau). \tag{9}$$

Here, $\{\mathbf{d}\}$ is a new set of unknown parameters to be evaluated, which indicates the contribution of the individual vibration modes for a particular vibration frequency. The space functions are completely known from the earlier static analysis and the set of temporal functions is expressed by $\gamma_i = e^{i\omega\tau}$, where ω represents the natural frequency of the system.

Using these dynamic displacement fields and putting Eqs. (2), (3), and (8) into Eq. (7), the governing equation of the dynamic problem can be written in the form

$$-\omega^2[\mathbf{M}]\{\mathbf{d}\}+[\mathbf{K}]\{\mathbf{d}\}=0, \tag{10}$$

where $[\mathbf{M}]$ is the mass matrix of dimension $(n_w+n_u+n_v)$ and its elements are as follows:

$$\begin{bmatrix} \mathbf{M}_{11} & \mathbf{0} & \mathbf{0} \\ \mathbf{0} & \mathbf{M}_{22} & \mathbf{0} \\ \mathbf{0} & \mathbf{0} & \mathbf{M}_{33} \end{bmatrix},$$

where

$$[\mathbf{M}_{11}]=\rho t\sum_{j=1}^{n_w}\sum_{i=1}^{n_w}\int_0^1\int_0^1 \phi_i\phi_j \det\mathbf{J}\,\mathrm{d}\xi\,\mathrm{d}\eta,$$

$$[\mathbf{M}_{22}]=\rho t\sum_{j=n_w+1}^{n_w+n_u}\sum_{i=n_w+1}^{n_w+n_u}\int_0^1\int_0^1 \alpha_{i-n_w}\alpha_{j-n_w} \det\mathbf{J}\,\mathrm{d}\xi\,\mathrm{d}\eta,$$

$$[\mathbf{M}_{33}]=\rho t\sum_{j=n_w+n_u+1}^{n_w+n_u+n_v}\sum_{i=n_w+n_u+1}^{n_w+n_u+n_v}\int_0^1\int_0^1 \beta_{i-n_w-n_u}\beta_{j-n_w-n_u} \det\mathbf{J}\,\mathrm{d}\xi\,\mathrm{d}\eta.$$

Table 1
Validation of the results for the first five linear dimensionless frequency parameters for a rhombic plate with all edges simply supported

θ (deg)	Mode	Present study	Ref. [15]
15	1	20.889	20.73
	2	48.213	48.11
	3	56.192	55.84
	4	79.159	78.79
	5	105.039	103.82
30	1	25.065	24.69
	2	52.629	52.56
	3	72.136	71.24
	4	83.960	83.39
	5	124.104	122.02
45	1	35.680	34.24
	2	66.266	66.11
	3	100.518	99.54
	4	109.139	106.10
	5	141.399	140.08
60	1	66.84	60.96
	2	104.954	104.51
	3	148.710	146.51
	4	196.152	195.30
	5	214.749	203.60

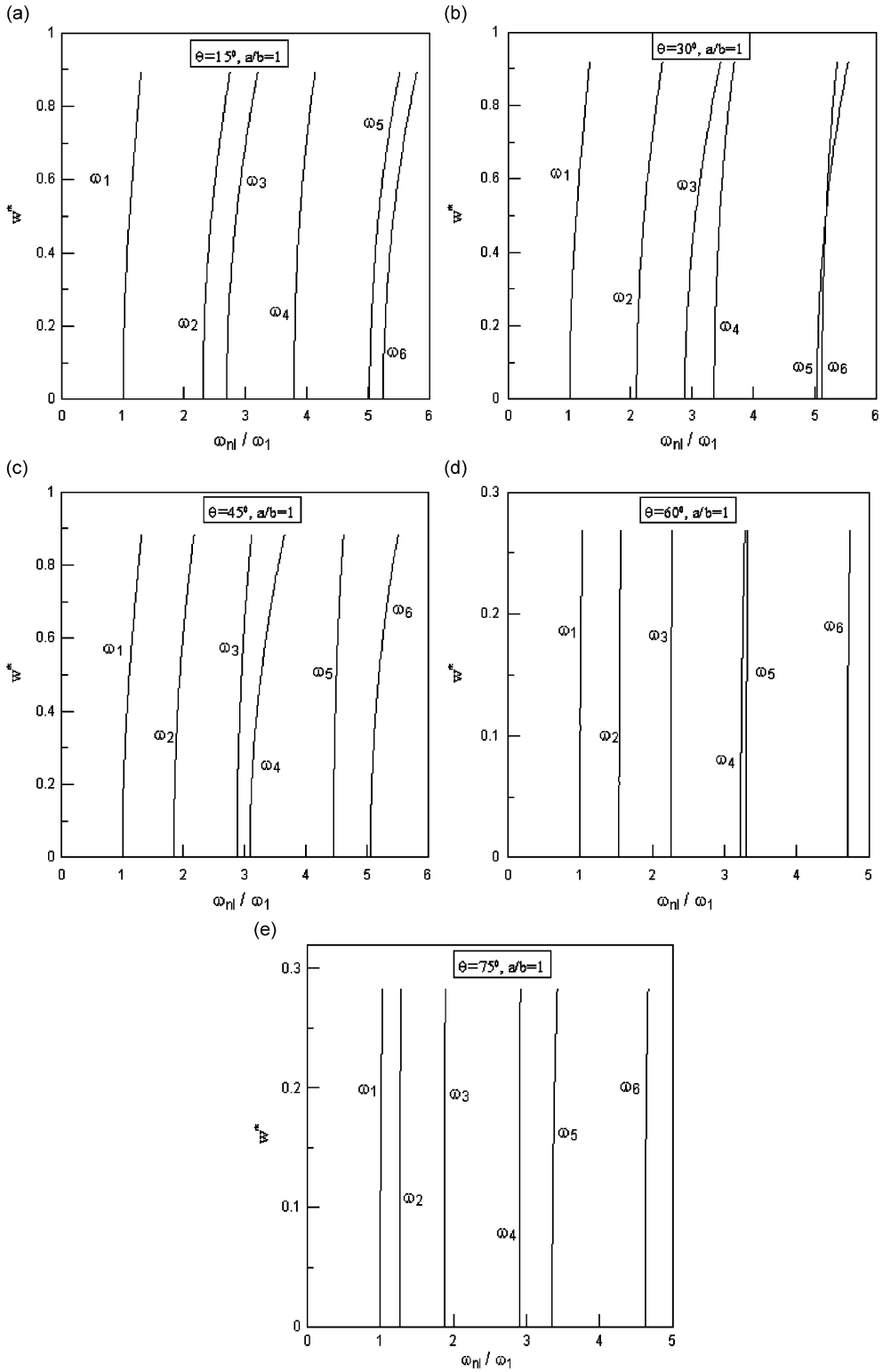

Fig. 3. Backbone curves for the SSSS skew plate for different skew angles with $a/b = 1$: (a) $\theta = 15^\circ$, (b) $\theta = 30^\circ$, (c) $\theta = 45^\circ$, (d) $\theta = 60^\circ$, and (e) $\theta = 75^\circ$.

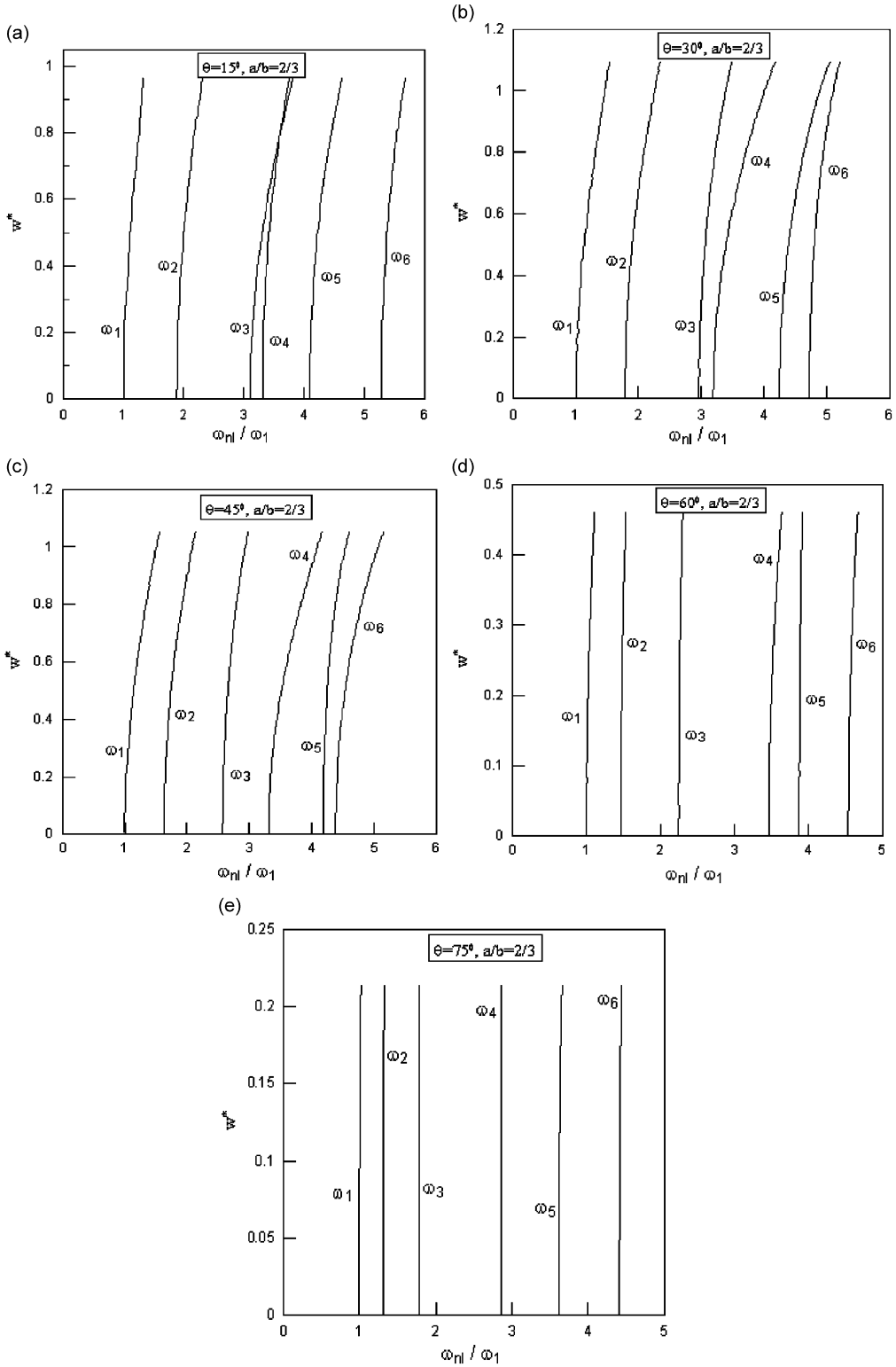

Fig. 4. Backbone curves for the SSSS skew plate for different skew angles with $a/b = 2/3$: (a) $\theta = 15^\circ$, (b) $\theta = 30^\circ$, (c) $\theta = 45^\circ$, (d) $\theta = 60^\circ$, and (e) $\theta = 75^\circ$.

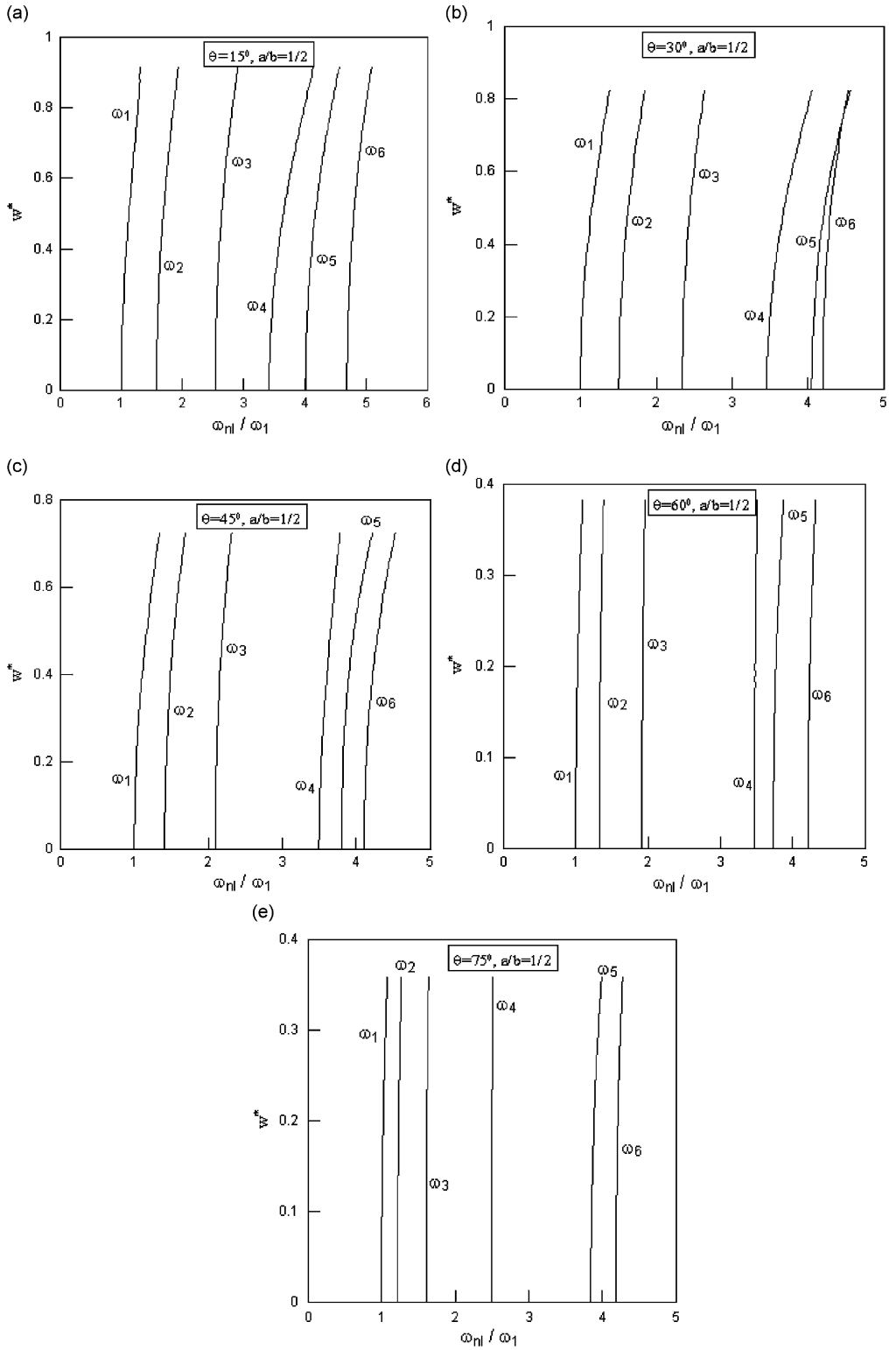

Fig. 5. Backbone curves for the SSSS skew plate for different skew angles with $a/b = 1/2$: (a) $\theta = 15^\circ$, (b) $\theta = 30^\circ$, (c) $\theta = 45^\circ$, (d) $\theta = 60^\circ$, and (e) $\theta = 75^\circ$.

Eq. (10) can be transformed to a standard eigenvalue problem by suitable rearrangement, which is solved numerically to calculate the natural frequencies using IMSL routines.

3. Results and discussions

The aim of this study is to investigate the effect of large deflection on the dynamic behaviour of skew plates and present its variation with different skew angles and aspect ratios. The analysis is based on calculating the static displacements of the plate and subsequently evaluating the eigenvalues of the corresponding dynamic

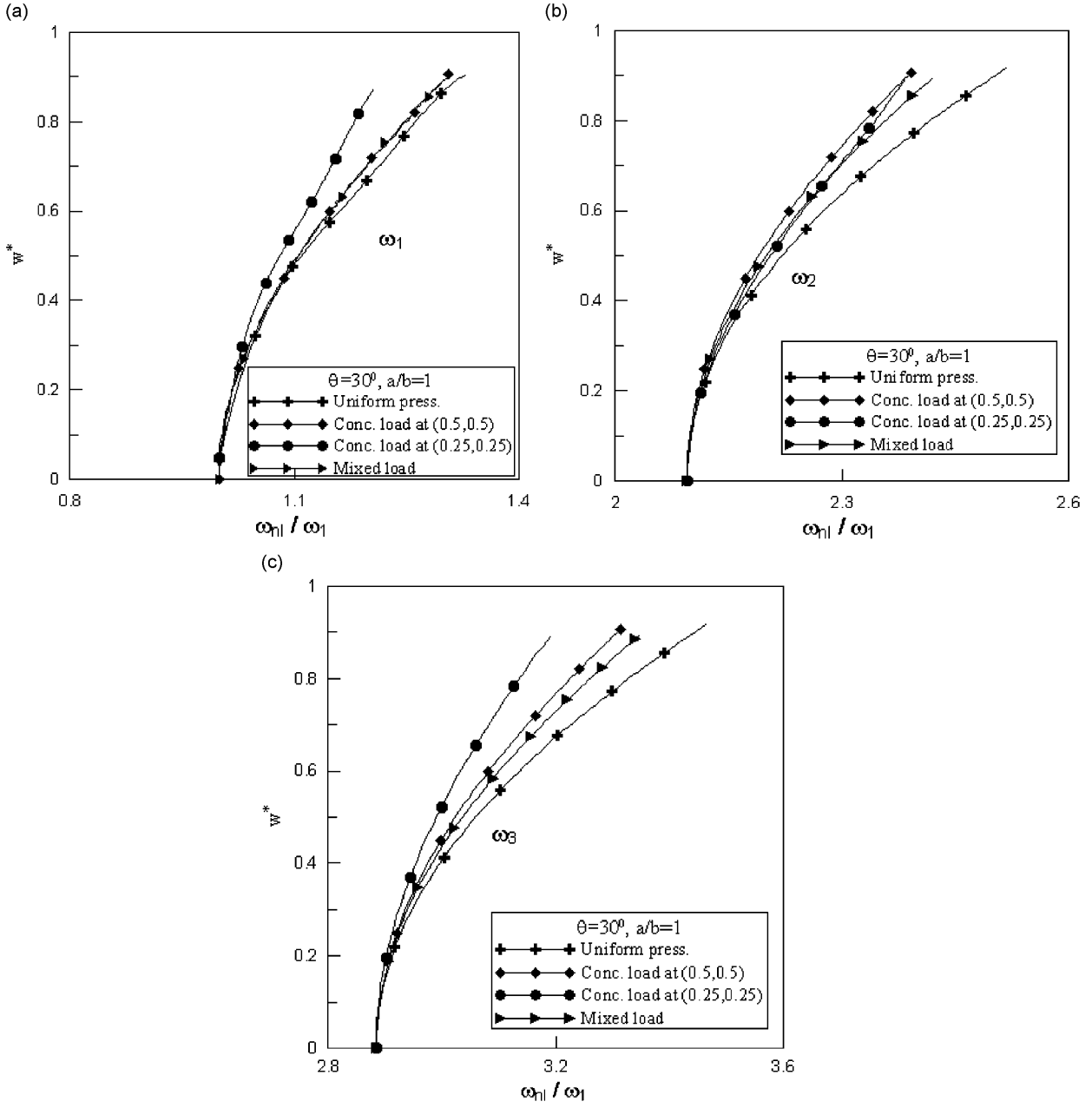

Fig. 6. Large-deflection dynamic behaviour for different types of loadings for the SSSS rhombic skew plate with $\theta = 30^{\circ}$: (a) Mode 1, (b) Mode 2, and (c) Mode 3.

problem formulated through the known displacement field. The square roots of these eigenvalues represent the free vibration frequencies of the skew plate at that deflected configuration. The displacement field corresponding to each of the eigenvalues provides the amplitude of free vibration.

The present method is quite general in nature so that it can be applied for any classical boundary condition. To keep the volume of the paper within reasonable limit, detailed results have only been presented for skew plates with all along simply supported boundaries (SSSS) where the static deflection in the plate is effected by uniform transverse pressure. However, some results for other type of loadings and boundary conditions have also been furnished to establish the generality and robustness of the present method. With regard to membrane effect, the edges of the plate are modeled as immovable by imposing zero in-plane displacement boundary conditions. The results are generated using the following material and geometric parameter values, $E = 210\,\text{GPa}$, $v = 1/3$, $a = 1.0\,\text{m}$, $\rho = 7850\,\text{kg}\,\text{m}^{-3}$, and $t = 0.01\,\text{m}$.

3.1. Validation

The linear dimensionless frequency parameter in line with an earlier research work [16] is defined as $\lambda = \omega a^2\sqrt{\rho t/D}$. In order to validate the present formulation, the first five linear dimensionless frequency

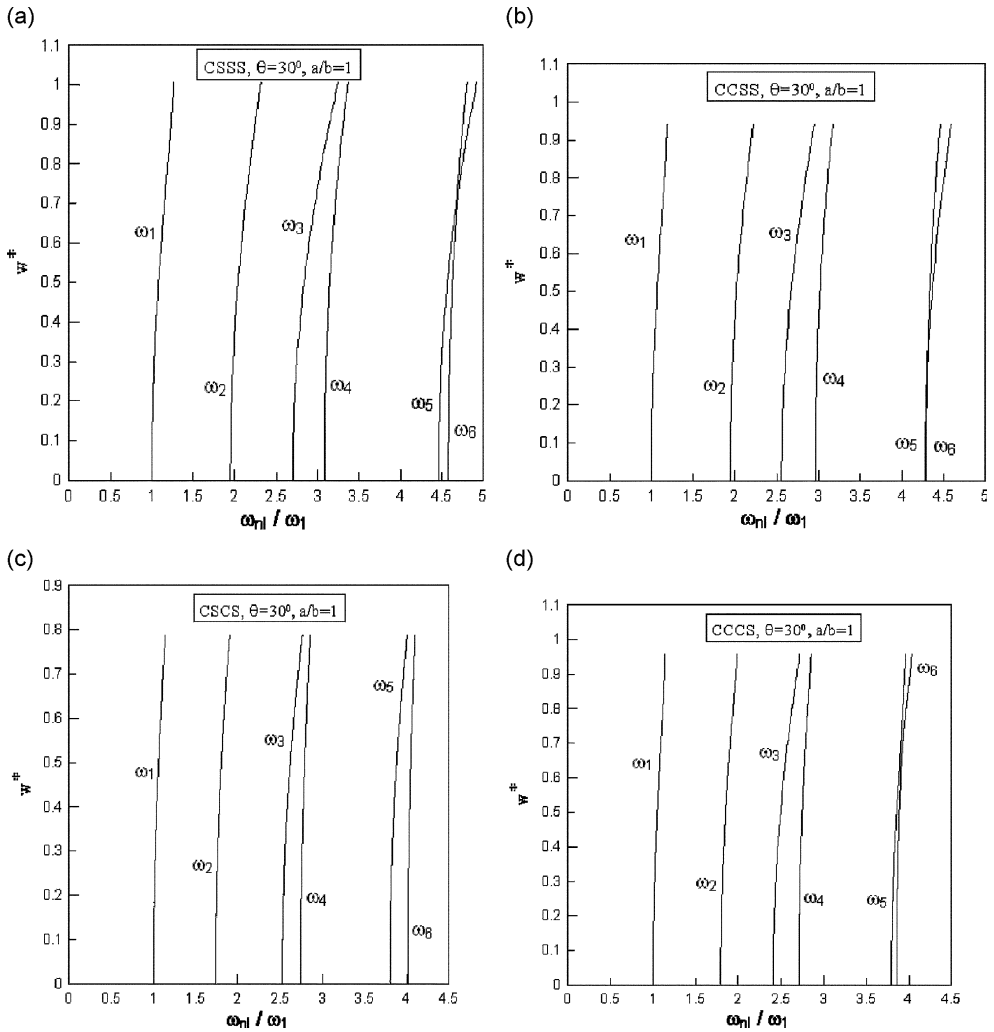

Fig. 7. Backbone curves for a rhombic skew plate with $\theta = 30^\circ$ having different boundary conditions: (a) CSSS, (b) CCSS, (c) CSCS, and (d) CCCS.

parameters for a rhombic plate with all edges simply supported for different skew angles have been compared with the corresponding results presented in Ref. [15] and it has been tabulated in Table 1. This table shows excellent agreement, thus establishing the validation of the present method. It should be mentioned that the results for calculating λ's as shown in Table 1 are generated by considering different number of functions for different skew angles. For $\theta = 15^\circ$, 30°, 45°, and 60°, numbers of functions for each plate displacements (w, u and v) are taken as $25(5 \times 5)$, $36(6 \times 6)$, $49(7 \times 7)$, and $64(8 \times 8)$, respectively, where numbers in the parentheses provide a break up for the order of the functions corresponding to two orthogonal directions. It is evident that the convergence is dependent on the number of functions for different skew angles.

3.2. Large-deflection dynamic behaviour of the SSSS skew plate under uniform pressure

The large-amplitude dynamic behaviour of a skew plate is shown graphically as the backbone curves for different skew angles in Figs. 3(a–e), 4(a–e), and 5(a–e) for different fixed values of aspect ratios (a/b). These backbone curves have been shown for the first six mode shapes in the dimensionless amplitude–frequency plane. The ratio of the maximum plate deflection to plate thickness is taken as the dimensionless amplitude w^* ($= w_{\max}/t$) while the dimensionless frequency ($\omega_{\mathrm{nl}}/\omega_1$) is obtained by normalizing the nonlinear frequency (ω_{nl}) with the corresponding fundamental linear frequency (ω_1). In Figs. 3–5, the aspect ratios are

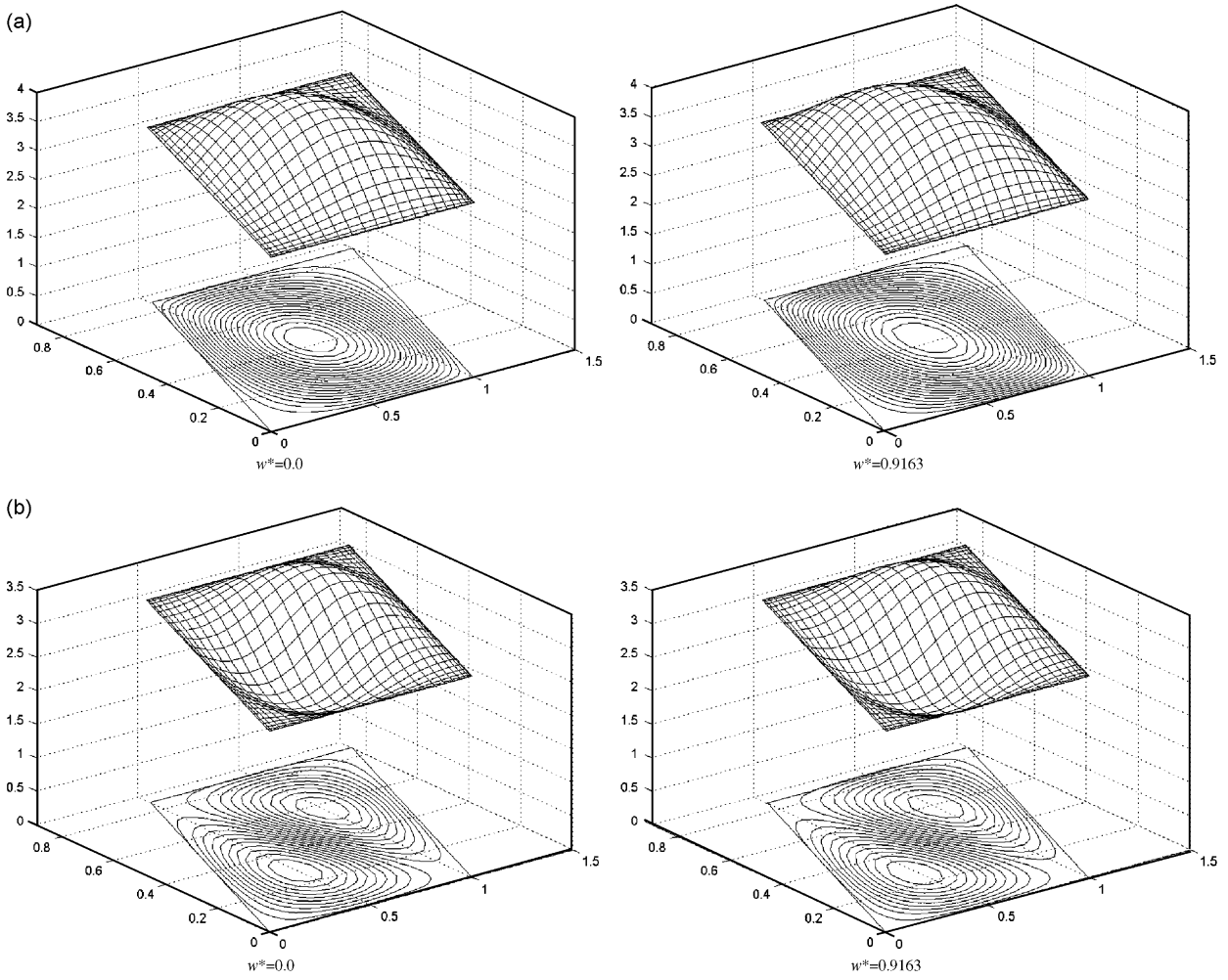

Fig. 8. Mode shape plots for an SSSS skew plate with $\theta = 30^\circ$ and $a/b = 1$ (corresponding to backbone curves in Fig. 3(b)): (a) Mode 1, (b) Mode 2, (c) Mode 3, (d) Mode 4, (e) Mode 5, and (f) Mode 6.

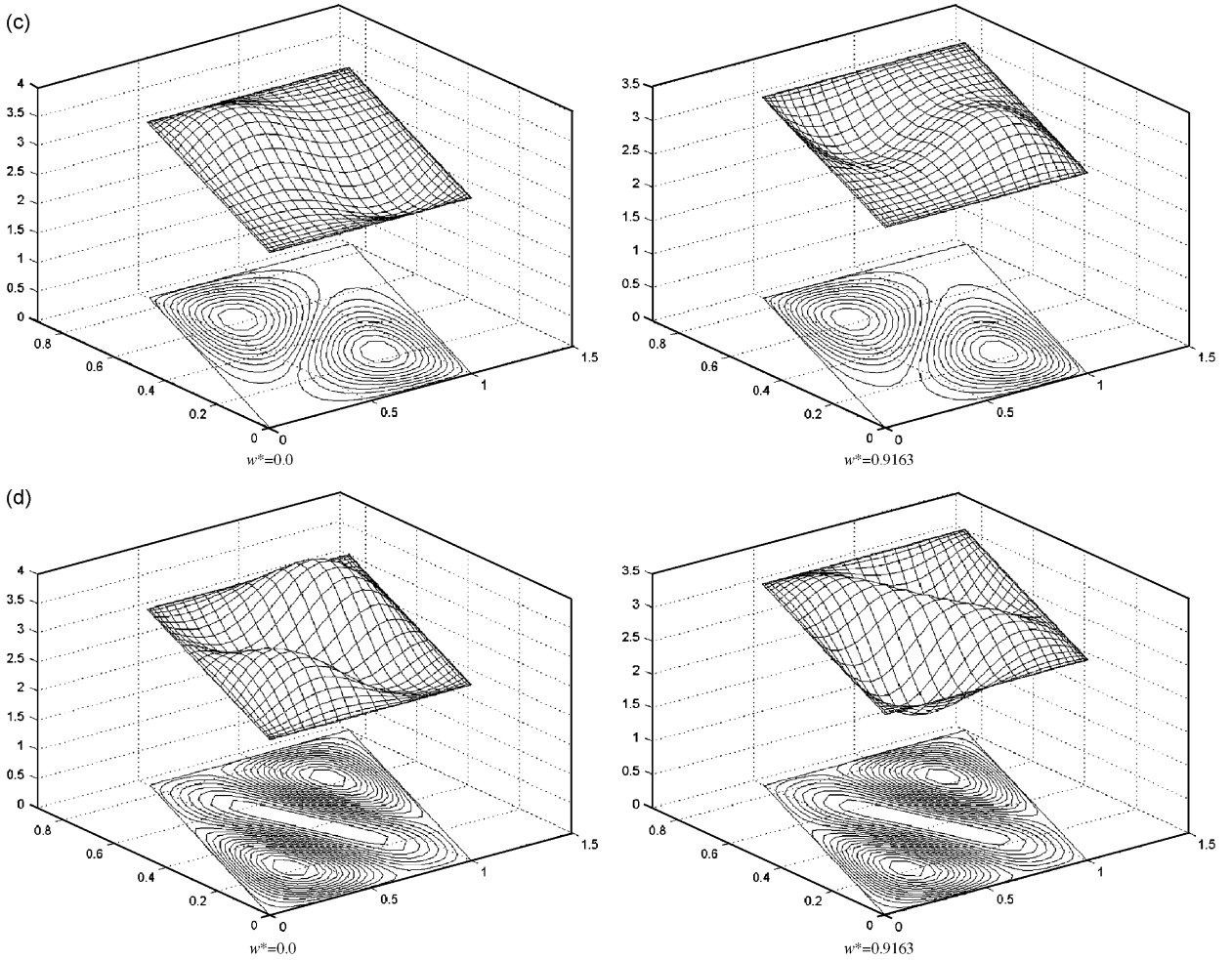

Fig. 8. (*Continued*)

taken as 1, 2/3, and 1/2, respectively, and corresponding to each of these aspect ratios, the variation in the dynamic behaviour of skew plates is shown for $\theta = 15^\circ$, 30°, 45°, 60°, and 75°. It must be noted that the number of functions for each computation is selected suitably for different skew angles. This is done to reduce the computational time because it increases exponentially with the number of functions. As mentioned earlier, obtaining convergence is much more problematic for larger skew angles and hence results for these cases are generated up to a lower value of w^*.

The general trend that can be obtained from any of the backbone curves is that the free vibration frequency increases as the deflection of the skew plate increases as can be seen from any of the plots of Figs. 3–5. The specific reason for this trend can be attributed to the fact that the plate stiffens with increase in deflection due to the effect of geometric nonlinearity, resulting in the increase in nonlinear frequency. This effect is apparently more pronounced for skew angles up to 45°. For skew angles 60° and above, the effect seems insignificant due to the difference in the dimensionless amplitude scale. This trend is consistent irrespective of the aspect ratios.

The phenomenon of mode switching has been observed for some specific geometry of skew plates. This phenomenon has been observed for $\theta = 30^\circ$, $a/b = 1$; $\theta = 15^\circ$, $a/b = 2/3$, and $\theta = 30^\circ$, $a/b = 1/2$ as can be seen from Figs. 3(b), 4(a), and 5(b), respectively. This is appropriately supported by mode shape plots presented in Section 3. It can be further seen from the figures that for $a/b = 1$ and $a/b = 1/2$, mode switching occurs between ω_5 and ω_6 (Figs. 3(b) and 5(b), respectively), whereas for $a/b = 2/3$, it occurs between ω_3 and

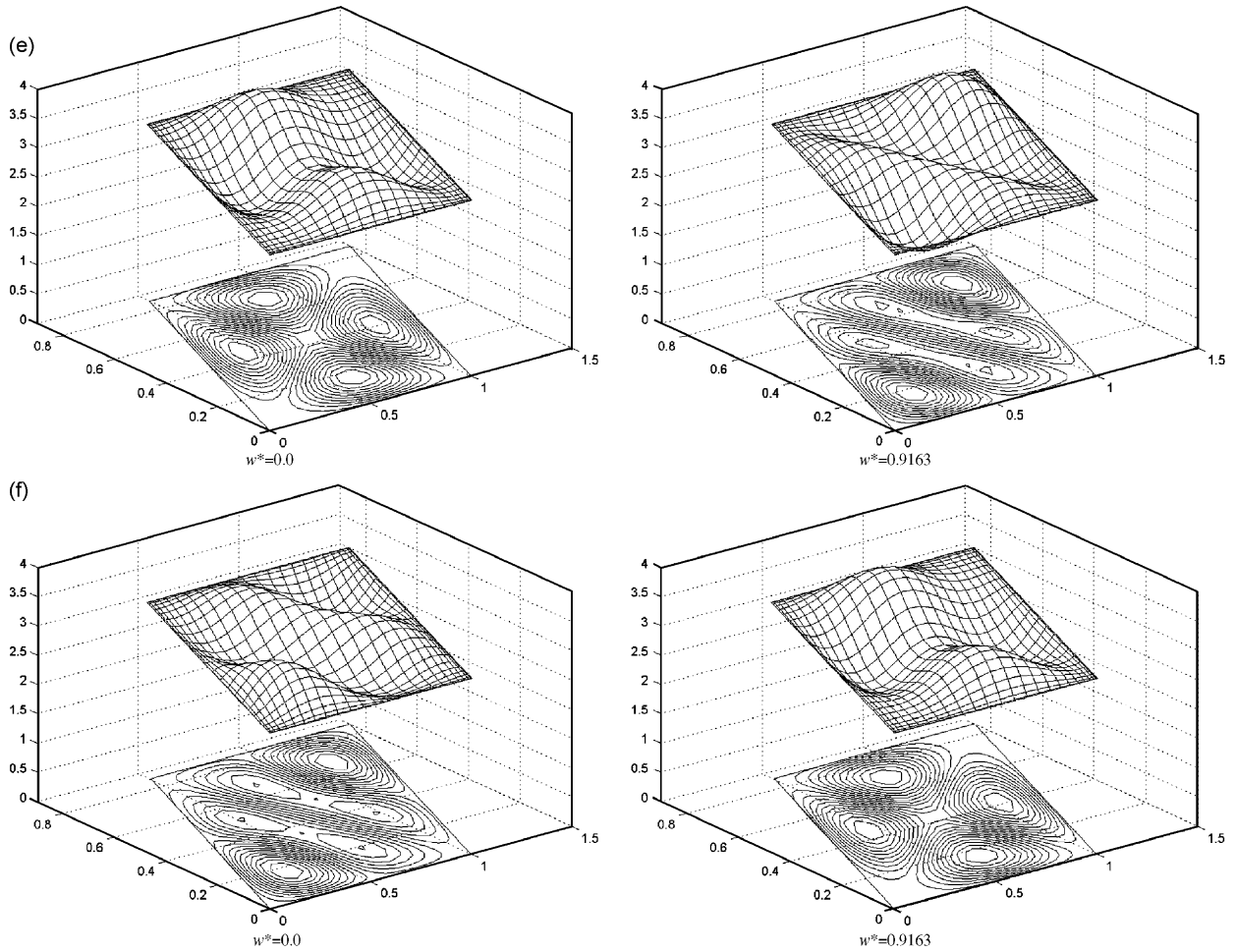

Fig. 8. (*Continued*)

ω_4 (Fig. 4(a)). It can be easily understood that the occurrence of mode switching is entirely system dependent and the modes between which switching occurs are also dependent on the corresponding system.

3.3. Results for other types of loadings and boundary conditions

In Section 3.2, results have been presented for uniform transverse pressure for SSSS skew plates. The present formulation is robust enough to take into account any type of loadings, be it uniform transverse pressure, or concentrated transverse loads at arbitrary locations or a combination of both to name a few. The effect of some different types of loadings on dynamic behaviour of skew plate has also been investigated in the present paper, which are (i) concentrated load at midpoint (0.5, 0.5), (ii) concentrated load at point (0.25, 0.25), and (iii) a combination of uniform transverse pressure and concentrated load at midpoint, termed as mixed load in the legends of the plots. The large-deflection dynamic behaviour for the SSSS rhombic skew plate ($a/b = 1$) with $\theta = 30^\circ$ for these three new types of loading along with the earlier one has been presented in the form of backbone curves in Figs. 6(a–c) for the first three vibration modes, respectively. The frequency of vibration increases monotonically with amplitude for all four types of loadings, but for uniform transverse pressure this increase is maximum. The combined concentrated and uniform pressure loading comes next in this respect and the effect of concentrated load alone on that particular behaviour is the least. The effect of

location of concentrated transverse load on the dynamic behaviour of skew plate is also prominent from Figs. 6(a–c) but further study is required to arrive at certain conclusions in this regard.

In order to check the robustness of the present formulation in terms of boundary conditions, the same is used to consider the dynamic behaviour of skew plates having mixed boundary conditions loaded with uniformly distributed transverse pressure. For this purpose, backbone curves for different combinations of clamped and simply supported edges (CSSS, CCSS, CSCS, and CCCS) for rhombic skew plates with $\theta = 30^\circ$ have been presented in Figs. 7(a–d), respectively, for the first six vibration modes. It should be noted that the letter 'C' denotes clamped boundary and the nomenclature of the boundary condition starts from the skew edge passing through the origin and proceed in the counter-clockwise direction. The dynamic behaviour as can be viewed from Fig. 7 remains same as that mentioned for the SSSS skew plate in Section 3.2. The mode switching phenomenon as observed in Figs. 7(a) and (b) is apparent and the fact has been confirmed by studying the backbone curves at higher magnification and investigating the corresponding mode shape plots.

3.4. Mode shape plots

Mode shape plots for the first six vibration modes of SSSS skew plates under uniform transverse pressure have been presented for two specific geometries: $\theta = 30^\circ$, $a/b = 1$, and $\theta = 15^\circ$, $a/b = 2/3$ in Figs. 8(a–f) and

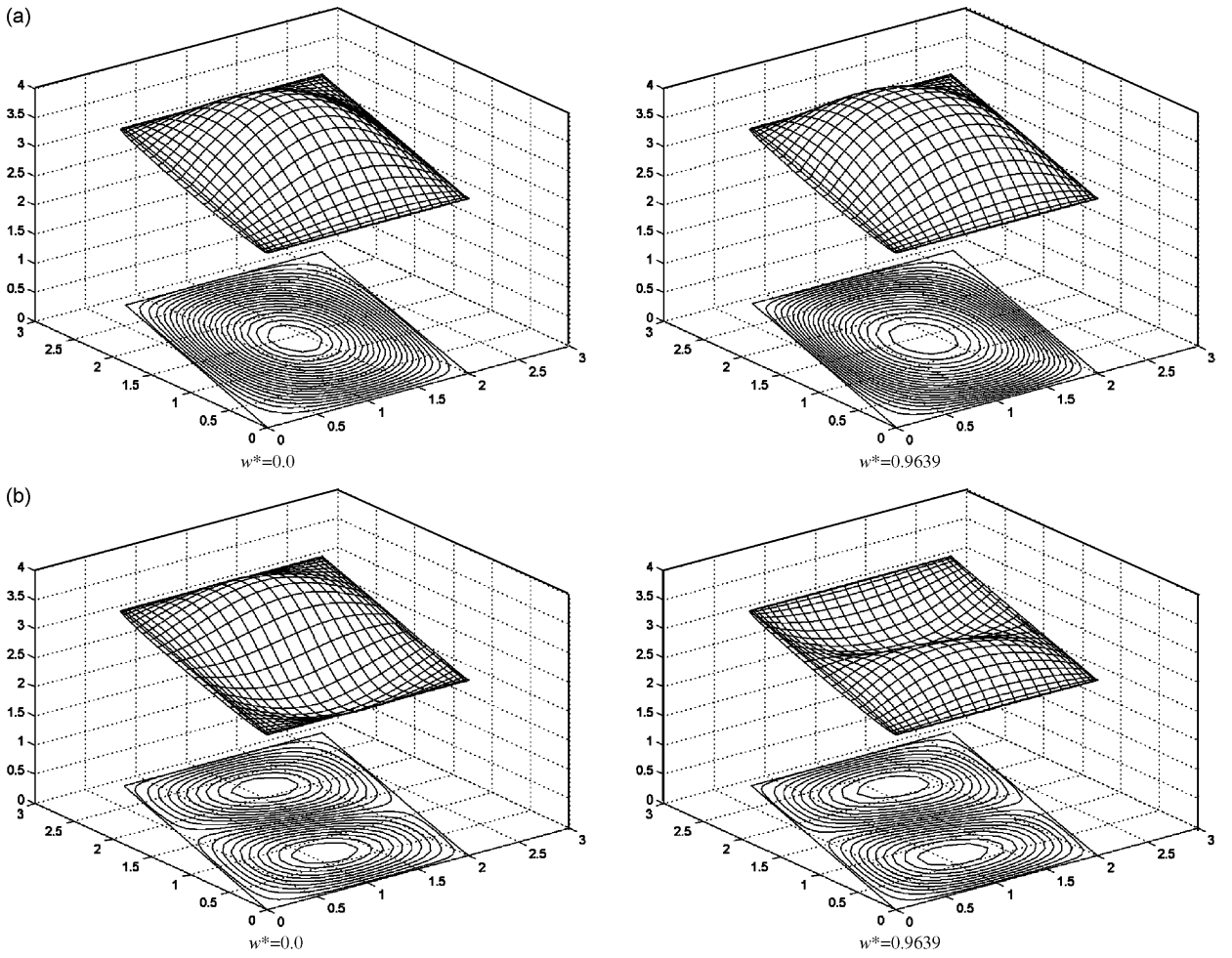

Fig. 9. Mode shape plots for an SSSS skew plate with $\theta = 15^\circ$ and $a/b = 2/3$ (corresponding to backbone curves in Fig. 4(a)): (a) Mode 1, (b) Mode 2, (c) Mode 3, (d) Mode 4, (e) Mode 5, and (f) Mode 6.

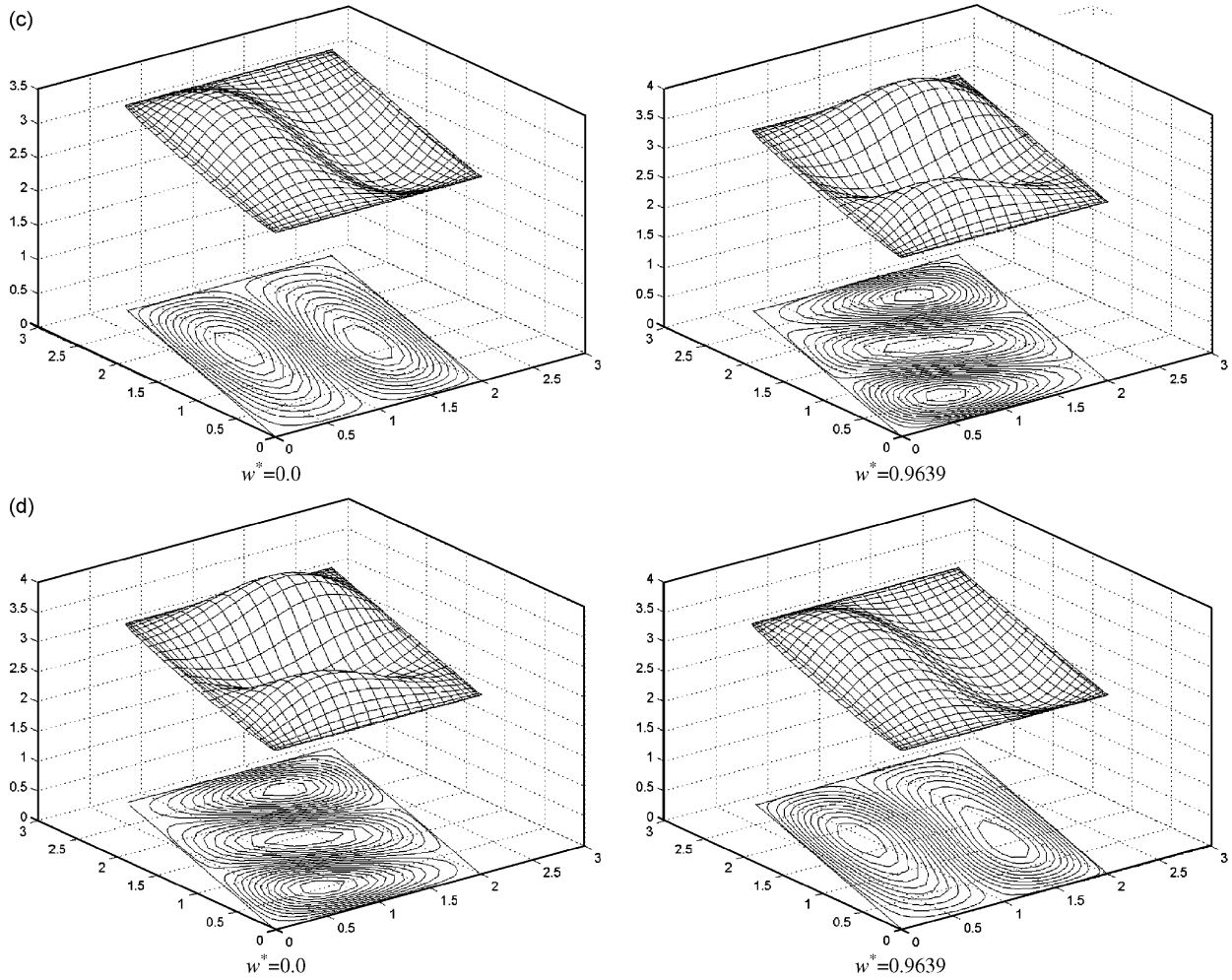

Fig. 9. (*Continued*)

9(a–f), respectively. For each mode of vibration, two mode shape plots corresponding to linear and nonlinear frequencies are given. The mode shape plots for nonlinear frequencies are given corresponding to the maximum deflected position up to which results have been generated. Also, it must be mentioned that the mode shape plots are presented for those geometries for which mode switching occurs, in order to visualize the phenomenon. In each plot, the surface plot and its corresponding contour plot for the vibrating skew plate have been presented. It is also to be noted that the amplitude of vibration for all the surface plots is scaled by the difference between the extremities of the displacement amplitude.

Although, it is apparent that the surface plots for a particular mode shape for linear and nonlinear frequencies for a particular aspect ratio and skew angle are identical in nature, a microlevel study reveals that their amplitude of vibration is different from each other. It is due to the fact that the amplitude of vibration depends on the corresponding static deflection of the skew plate. The microlevel observations are not presented here to maintain brevity.

The vibration mode shapes are also a function of the nature of loading, and to highlight the effect, sectional views of the mode shapes at large-amplitude have been presented in Figs. 10(a–c). These three figures correspond to the first three vibration modes of an SSSS rhombic skew plate with $\theta = 30^\circ$ for different types of loadings as considered earlier in Fig. 6. Two sections, one parallel to the x-axis and the other parallel to the skew edge, have been taken for each vibration mode. The section planes are so selected as to avoid the nodal

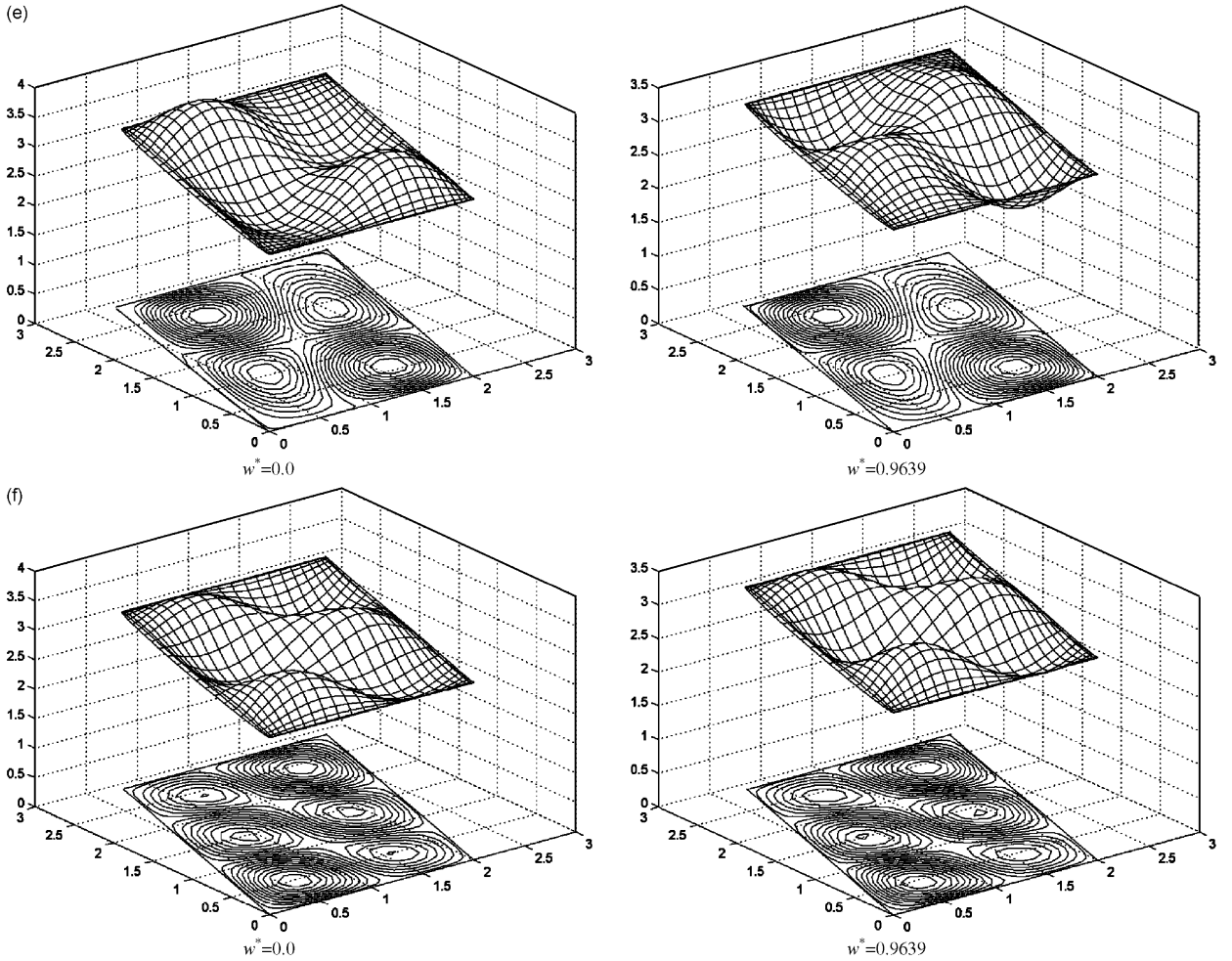

Fig. 9. (*Continued*)

points and their locations have been indicated in the legends of the figures. It must be noted that Figs. 10(a–c) are captured at $w^* = 0.8$. Fig. 10 clearly shows that vibration mode shapes depend on the nature of loading. Concentrated load at (0.25, 0.25) produces appreciable difference in its large-amplitude mode shapes from that obtained by the three other types of loadings because of its off-centred nature compared to the other three.

4. Conclusions

In this paper, the simulation model for large-amplitude free vibration analysis of thin isotropic skew plates subjected to uniform static pressure with all along simply supported flexural boundary conditions and immovable in-plane boundary conditions has been presented. The mathematical formulation is based on the variational form of the total potential energy of the system. The results are validated successfully with the available results. The dynamic behaviour of skew plates has been presented in the form of backbone curves in a dimensionless frequency–amplitude plane. The effect of different types of loadings and combination of clamped and simply supported boundary conditions have also been investigated. The mode shape plots are presented to visually differentiate between the linear and nonlinear dynamic behaviour of skew plates.

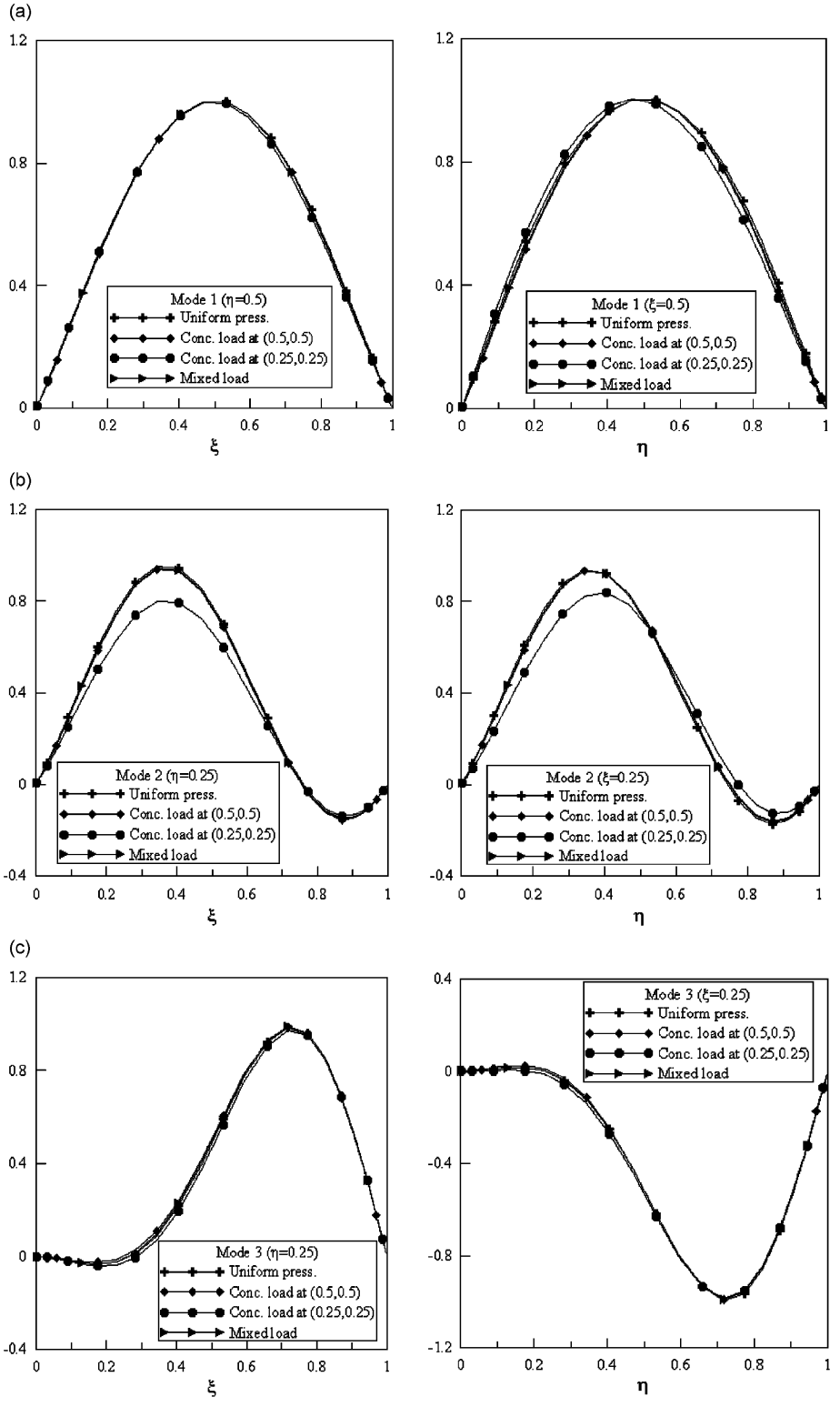

Fig. 10. Sectional views of large-amplitude vibration mode shapes for an SSSS rhombic skew plate with $\theta = 30^{\circ}$: (a) Mode 1, (b) Mode 2, and (c) Mode 3.

Acknowledgements

We acknowledge the comments and suggestions of the referees that have been instrumental in improving the paper in its final version.

Appendix. Details of matrix elements

Total stiffness matrix $[\mathbf{K}] = [\mathbf{k}^b] + [\mathbf{k}^m]$.

The form of $[\mathbf{k}^b]$ is given below:

$$[\mathbf{k}^b] = \begin{bmatrix} \mathbf{k}^b_{11} & \mathbf{k}^b_{12} & \mathbf{k}^b_{13} \\ \mathbf{k}^b_{21} & \mathbf{k}^b_{22} & \mathbf{k}^b_{23} \\ \mathbf{k}^b_{31} & \mathbf{k}^b_{32} & \mathbf{k}^b_{33} \end{bmatrix},$$

where

$$[\mathbf{k}^b_{11}] = D\sum_{j=1}^{n_w}\sum_{i=1}^{n_w}\int_0^1\int_0^1\left[\left\{\left(\frac{\partial^2\phi_i}{\partial x^2}\right)\left(\frac{\partial^2\phi_j}{\partial x^2}\right)+\left(\frac{\partial^2\phi_i}{\partial y^2}\right)\left(\frac{\partial^2\phi_j}{\partial y^2}\right)+\left(\frac{\partial^2\phi_i}{\partial y^2}\right)\left(\frac{\partial^2\phi_j}{\partial x^2}\right)+\left(\frac{\partial^2\phi_i}{\partial x^2}\right)\left(\frac{\partial^2\phi_j}{\partial y^2}\right)\right\}\right.$$
$$\left.-(1-\nu)\left\{\left(\frac{\partial^2\phi_i}{\partial y^2}\right)\left(\frac{\partial^2\phi_j}{\partial x^2}\right)+\left(\frac{\partial^2\phi_i}{\partial x^2}\right)\left(\frac{\partial^2\phi_j}{\partial y^2}\right)-2\left(\frac{\partial^2\phi_i}{\partial x\,\partial y}\right)\left(\frac{\partial^2\phi_j}{\partial x\,\partial y}\right)\right\}\right]\det\mathbf{J}\,\mathrm{d}\xi\,\mathrm{d}\eta$$

and $[\mathbf{k}^b_{12}] = [\mathbf{k}^b_{13}] = [\mathbf{k}^b_{21}] = [\mathbf{k}^b_{22}] = [\mathbf{k}^b_{23}] = [\mathbf{k}^b_{31}] = [\mathbf{k}^b_{32}] = [\mathbf{k}^b_{33}] = \mathbf{0}$.

The form of $[\mathbf{k}^m]$ is

$$[\mathbf{k}^m] = \begin{bmatrix} \mathbf{k}^m_{11} & \mathbf{k}^m_{12} & \mathbf{k}^m_{13} \\ \mathbf{k}^m_{21} & \mathbf{k}^m_{22} & \mathbf{k}^m_{23} \\ \mathbf{k}^m_{31} & \mathbf{k}^m_{32} & \mathbf{k}^m_{33} \end{bmatrix},$$

where

$$[\mathbf{k}^m_{11}] = \frac{Et}{2(1-\nu^2)}\sum_{j=1}^{n_w}\sum_{i=1}^{n_w}\int_0^1\int_0^1\left[\left(\sum_{i=1}^{n_w}d_i\frac{\partial\phi_i}{\partial x}\right)^2\frac{\partial\phi_i}{\partial x}\frac{\partial\phi_j}{\partial x}+\left(\sum_{i=1}^{n_w}d_i\frac{\partial\phi_i}{\partial y}\right)^2\frac{\partial\phi_i}{\partial y}\frac{\partial\phi_j}{\partial y}\right.$$
$$+\left(\sum_{i=1}^{n_w}d_i\frac{\partial\phi_i}{\partial x}\right)\left(\sum_{i=1}^{n_w}d_i\frac{\partial\phi_i}{\partial y}\right)\left\{\frac{\partial\phi_i}{\partial x}\frac{\partial\phi_j}{\partial y}+\frac{\partial\phi_i}{\partial y}\frac{\partial\phi_j}{\partial x}\right\}+(1-\nu)\left(\sum_{i=n_w+1}^{n_w+n_u}d_i\frac{\partial\alpha_{i-n_w}}{\partial y}\right)\frac{\partial\phi_i}{\partial x}\frac{\partial\phi_j}{\partial y}$$
$$\left.+(1-\nu)\left(\sum_{i=n_w+n_u+1}^{n_w+n_u+n_v}d_i\frac{\partial\beta_{i-n_w-n_u}}{\partial x}\right)\frac{\partial\phi_i}{\partial x}\frac{\partial\phi_j}{\partial y}\right]\det\mathbf{J}\,\mathrm{d}\xi\,\mathrm{d}\eta,$$

$$[\mathbf{k}^m_{12}] = \frac{Et}{2(1-\nu^2)}\sum_{j=1}^{n_w}\sum_{i=n_w+1}^{n_w+n_u}\int_0^1\int_0^1\left[2\left(\sum_{i=1}^{n_w}d_i\frac{\partial\phi_i}{\partial x}\right)\frac{\partial\alpha_{i-n_w}}{\partial x}\frac{\partial\phi_j}{\partial x}+2\nu\left(\sum_{i=1}^{n_w}d_i\frac{\partial\phi_i}{\partial y}\right)\frac{\partial\alpha_{i-n_w}}{\partial x}\frac{\partial\phi_j}{\partial y}\right.$$
$$\left.+(1-\nu)\left(\sum_{i=1}^{n_w}d_i\frac{\partial\phi_i}{\partial y}\right)\frac{\partial\alpha_{i-n_w}}{\partial y}\frac{\partial\phi_j}{\partial x}\right]\det\mathbf{J}\,\mathrm{d}\xi\,\mathrm{d}\eta,$$

$$[\mathbf{k}^m_{13}] = \frac{Et}{2(1-\nu^2)}\sum_{j=1}^{n_w}\sum_{i=n_w+n_u+1}^{n_w+n_u+n_v}\int_0^1\int_0^1\left[2\left(\sum_{i=1}^{n_w}d_i\frac{\partial\phi_i}{\partial y}\right)\frac{\partial\beta_{i-n_w-n_u}}{\partial y}\frac{\partial\phi_j}{\partial y}+2\nu\left(\sum_{i=1}^{n_w}d_i\frac{\partial\phi_i}{\partial x}\right)\frac{\partial\beta_{i-n_w-n_u}}{\partial y}\frac{\partial\phi_j}{\partial x}\right.$$
$$\left.+(1-\nu)\left(\sum_{i=1}^{n_w}d_i\frac{\partial\phi_i}{\partial y}\right)\frac{\partial\beta_{i-n_w-n_u}}{\partial x}\frac{\partial\phi_j}{\partial x}\right]\det\mathbf{J}\,\mathrm{d}\xi\,\mathrm{d}\eta,$$

$$[\mathbf{k}_{21}^m] = \frac{Et}{2(1-\nu^2)} \sum_{j=n_w+1}^{n_w+n_u} \sum_{i=1}^{n_w} \int_0^1 \int_0^1 \left[2\left(\sum_{i=1}^{n_w} d_i \frac{\partial \phi_i}{\partial x} \right) \frac{\partial \phi_i}{\partial x} \frac{\partial \alpha_{j-n_w}}{\partial x} + \nu \left(\sum_{i=1}^{n_w} d_i \frac{\partial \phi_i}{\partial y} \right) \frac{\partial \phi_i}{\partial y} \frac{\partial \alpha_{j-n_w}}{\partial x} + (1-\nu) \left(\sum_{i=1}^{n_w} d_i \frac{\partial \phi_i}{\partial x} \right) \frac{\partial \phi_i}{\partial y} \frac{\partial \alpha_{j-n_w}}{\partial y} \right] \det \mathbf{J} \, \mathrm{d}\xi \, \mathrm{d}\eta,$$

$$[\mathbf{k}_{22}^m] = \frac{Et}{2(1-\nu^2)} \sum_{j=n_w+1}^{n_w+n_u} \sum_{i=n_w+1}^{n_w+n_u} \int_0^1 \int_0^1 \left[2 \frac{\partial \alpha_{i-n_w}}{\partial x} \frac{\partial \alpha_{j-n_w}}{\partial x} + (1-\nu) \frac{\partial \alpha_{i-n_w}}{\partial y} \frac{\partial \alpha_{j-n_w}}{\partial y} \right] \det \mathbf{J} \, \mathrm{d}\xi \, \mathrm{d}\eta,$$

$$[\mathbf{k}_{23}^m] = \frac{Et}{2(1-\nu^2)} \sum_{j=n_w+1}^{n_w+n_u} \sum_{i=n_w+n_u+1}^{n_w+n_u+n_v} \int_0^1 \int_0^1 \left[2\nu \frac{\partial \beta_{i-n_w-n_u}}{\partial y} \frac{\partial \alpha_{j-n_w}}{\partial x} + (1-\nu) \frac{\partial \beta_{i-n_w-n_u}}{\partial x} \frac{\partial \alpha_{j-n_w}}{\partial y} \right] \det \mathbf{J} \, \mathrm{d}\xi \, \mathrm{d}\eta.$$

$$[\mathbf{k}_{31}^m] = \frac{Et}{2(1-\nu^2)} \sum_{j=n_w+n_u+1}^{n_w+n_u+n_v} \sum_{i=1}^{n_w} \int_0^1 \int_0^1 \left[2\left(\sum_{i=1}^{n_w} d_i \frac{\partial \phi_i}{\partial y} \right) \frac{\partial \phi_i}{\partial y} \frac{\partial \beta_{j-n_w-n_u}}{\partial y} + \nu \left(\sum_{i=1}^{n_w} d_i \frac{\partial \phi_i}{\partial x} \right) \frac{\partial \phi_i}{\partial x} \frac{\partial \beta_{j-n_w-n_u}}{\partial y} + (1-\nu) \left(\sum_{i=1}^{n_w} d_i \frac{\partial \phi_i}{\partial x} \right) \frac{\partial \phi_i}{\partial y} \frac{\partial \beta_{j-n_w-n_u}}{\partial x} \right] \det \mathbf{J} \, \mathrm{d}\xi \, \mathrm{d}\eta,$$

$$[\mathbf{k}_{32}^m] = \frac{Et}{2(1-\nu^2)} \sum_{j=n_w+n_u+1}^{n_w+n_u+n_v} \sum_{i=n_w+1}^{n_w+n_u} \int_0^1 \int_0^1 \left[2\nu \frac{\partial \alpha_{i-n_w}}{\partial x} \frac{\partial \beta_{j-n_w-n_u}}{\partial y} + (1-\nu) \frac{\partial \alpha_{i-n_w}}{\partial y} \frac{\partial \beta_{j-n_w-n_u}}{\partial x} \right] \det \mathbf{J} \, \mathrm{d}\xi \, \mathrm{d}\eta,$$

$$[\mathbf{k}_{33}^m] = \frac{Et}{2(1-\nu^2)} \sum_{j=n_w+n_u+1}^{n_w+n_u+n_v} \sum_{i=n_w+n_u+1}^{n_w+n_u+n_v} \int_0^1 \int_0^1 \left[2 \frac{\partial \beta_{i-n_w-n_u}}{\partial y} \frac{\partial \beta_{j-n_w-n_u}}{\partial y} + (1-\nu) \frac{\partial \beta_{i-n_w-n_u}}{\partial x} \frac{\partial \beta_{j-n_w-n_u}}{\partial x} \right] \det \mathbf{J} \, \mathrm{d}\xi \, \mathrm{d}\eta.$$

The load vector $\{\mathbf{f}\}$ is of the form $[\mathbf{f}_{11} \quad \mathbf{f}_{12} \quad \mathbf{f}_{13}]^{\mathrm{T}}$,where

$$\{\mathbf{f}_{11}\} = p \sum_{j=1}^{n_w} \int_0^1 \int_0^1 \phi_j \det \mathbf{J} \, \mathrm{d}\xi \, \mathrm{d}\eta + P\phi_j|_{\xi,\eta}$$

and $\{\mathbf{f}_{12}\} = \{\mathbf{f}_{13}\} = \mathbf{0}$, as there is no contribution of in-plane loading.

Here, $\mathbf{J}$ is the Jacobian of the transformation from the $x-y$ plane to the $\xi-\eta$ plane given by

$$\mathbf{J} = \begin{bmatrix} \left(\dfrac{\partial x}{\partial \xi}\right) & \left(\dfrac{\partial y}{\partial \xi}\right) \\ \left(\dfrac{\partial x}{\partial \eta}\right) & \left(\dfrac{\partial y}{\partial \eta}\right) \end{bmatrix}.$$

The details of the Jacobian are available in Ref. [18].

References

[1] G. Prathap, T.K. Varadan, Non-linear flexural vibrations of anisotropic skew plates, *Journal of Sound and Vibration* 63 (3) (1979) 315–323.

[2] K.M. Liew, K.Y. Lam, Application of two-dimensional orthogonal plate function to flexural vibration of skew plates, *Journal of Sound and Vibration* 139 (2) (1990) 241–252.

[3] O.G. McGee, W.D. Graves, T.S. Butalia, M.I. Owings, Natural vibrations of shear deformable rhombic plates with clamped and free edge conditions, *Computers and Structures* 53 (3) (1994) 679–694.

[4] B. Singh, S. Chakraverty, Flexural vibration of skew plates using boundary characteristic orthogonal polynomials in two variables, *Journal of Sound and Vibration* 173 (2) (1994) 157–178.

[5] S. Wang, Free vibration analysis of skew fibre-reinforced composite laminates based on first-order shear deformation plate theory, *Computers and Structures* 63 (3) (1997) 525–538.

[6] B. Singh, V. Saxena, Transverse vibration of skew plates with variable thickness, *Journal of Sound and Vibration* 206 (1) (1997) 1–13.

[7] P. Žitňan, Vibration analysis of rectangular and skew plates by the Rayleigh–Ritz method, *Journal of Sound and Vibration* 221 (2) (1999) 342–349.
[8] A.R.K. Reddy, R. Palaninathan, Free vibration of skew laminates, *Computers and Structures* 70 (4) (1999) 415–423.
[9] M.M. Saadatpour, M. Azhari, M.A. Bradford, Vibration analysis of simply supported plates of general shape with internal point and line supports using the Galerkin method, *Engineering Structures* 22 (9) (2000) 1180–1188.
[10] T. Mizusawa, K. Kondo, Application of the spline element method to analyze vibration of skew Mindlin plates with varying thickness in one direction, *Journal of Sound and Vibration* 241 (3) (2001) 485–501.
[11] M.K. Singha, M. Ganapathi, Large amplitude free flexural vibrations of laminated composite skew plates, *International Journal of Non-Linear Mechanics* 39 (2004) 1709–1720.
[12] K.M. Liew, J. Wang, T.Y. Ng, M.J. Tan, Free vibration and buckling analyses of shear-deformable plates based on FSDT meshfree method, *Journal of Sound and Vibration* 276 (2004) 997–1017.
[13] P. Malekzadeh, G. Karami, Polynomial and harmonic differential quadrature methods for free vibration of variable thickness thick skew plates, *Engineering Structures* 27 (2005) 1563–1574.
[14] D. Zhou, S.H. Lo, F.T.K. Au, Y.K. Cheung, W.Q. Liu, 3-D vibration analysis of skew thick plates using Chebyshev–Ritz method, *International Journal of Mechanical Sciences* 48 (12) (2006) 1481–1493.
[15] A.V. Singh, M. Tanveer, Eigenvalue analysis of doubly connected plates with different configurations, *Journal of Sound and Vibration* 295 (2006) 76–93.
[16] K.N. Saha, D. Misra, G. Pohit, S. Ghosal, Large amplitude free vibration study of square plates under different boundary conditions through a static analysis, *Journal of Vibration and Control* 10 (2004) 1009–1028.
[17] R.D. Cook, D.S. Malkus, M.E. Plesha, *Concepts and Applications of Finite Element Analysis*, Wiley, USA, 1989.
[18] A.V. Singh, Y. Elaghabash, On the finite displacement analysis of quadrangular plates, *International Journal of Non-Linear Mechanics* 38 (2003) 1149–1162.